

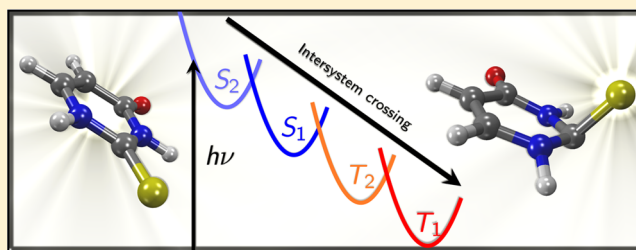
# A Static Picture of the Relaxation and Intersystem Crossing Mechanisms of Photoexcited 2-Thiouracil

Sebastian Mai, Philipp Marquetand,\* and Leticia González\*

Institute of Theoretical Chemistry, University of Vienna, Währinger Straße 17, 1090 Vienna, Austria

## Supporting Information

**ABSTRACT:** Accurate excited-state quantum chemical calculations on 2-thiouracil, employing large active spaces and up to quadruple- $\zeta$  quality basis sets in multistate complete active space perturbation theory calculations, are reported. The results suggest that the main relaxation path for 2-thiouracil after photoexcitation should be  $S_2 \rightarrow S_1 \rightarrow T_2 \rightarrow T_1$ , and that this relaxation occurs on a subpicosecond time scale. There are two deactivation pathways from the initially excited bright  $S_2$  state to  $S_1$ , one of which is nearly barrierless and should promote ultrafast internal conversion. After relaxation to the  $S_1$  minimum, small singlet–triplet energy gaps and spin–orbit couplings of about  $130 \text{ cm}^{-1}$  are expected to facilitate intersystem crossing to  $T_2$ , from where very fast internal conversion to  $T_1$  occurs. An important finding is that 2-thiouracil shows strong pyramidalization at the carbon atom of the thiocarbonyl group in several excited states.



## INTRODUCTION

Nucleobase analogues, which are structurally similar to the canonical nucleobases adenine, guanine, cytosine, uracil, and thymine, play an important role in biochemistry. Many nucleobase analogues are actively used as drugs for chemotherapy<sup>1</sup> and various other diseases or as fluorescence markers<sup>2–4</sup> in biomolecular research. Oftentimes, the close structural relation to the parent nucleobases is responsible for the usefulness of a given nucleobase analogue. For example, many nucleobase analogues can substitute the canonical nucleobases in DNA and thus affect the properties of DNA. Despite this structural similarity, the photochemical properties of nucleobase analogues can drastically differ from the ones of their parent nucleobases. The canonical nucleobases are known to exhibit ultrafast relaxation to the ground state after irradiation with UV light, which gives DNA a high stability against UV-induced damage.<sup>5–7</sup> In contrast, for a large number of nucleobase analogues,<sup>8–11</sup> slow internal conversion to the ground state, luminescence, and intersystem crossing is reported. This difference is correlated with the fact that the excited-state potential energy surfaces (PES) are sensitive to the functionalization of the molecule and even small changes in the relative energies of the PES can lead to drastically different excited-state dynamics. For this reason, the incorporation of nucleobase analogues into DNA can severely affect its photostability.

Thiated nucleobases (thiobases), where one or more oxygen atoms of a canonical nucleobase are exchanged for sulfur, are a very good example of the above-described behavior. Thiobases are found in several types of RNA<sup>12</sup> but also have been employed as drugs. For example, 6-thioguanine (6TG) is a very important cancer and anti-inflammatory drug, listed as an essential medicine by the WHO.<sup>13</sup> Interestingly, a side effect of 6TG treatment is an

100-fold increase in the incidence of skin cancer,<sup>14</sup> which has been attributed to its very different photochemistry<sup>15–19</sup> in comparison with guanine. Similarly, 2-thiouracil (2TU) has been historically used as an antithyroid drug (6-*n*-propyl-2-thiouracil<sup>20</sup> is currently listed as essential by the WHO<sup>13</sup>) and has shown some potential for the development of cytostatica,<sup>21</sup> heavy-metal antidotes,<sup>22</sup> or photosensitizers for photodynamical therapy.<sup>23</sup> As with 6TG, the different photophysics and photochemistry of 2TU in comparison with uracil could lead to significant side effects in potential medical applications of 2TU. This relevance has led to an increased interest in the photophysics of thiobases.

The UV absorption spectrum and excited states of 2TU have been studied in detail. The first band of the UV absorption spectrum has a maximum at approximately 270 nm, with the band extending to about 350 nm.<sup>24,25</sup> Additionally, this band shows either a shoulder or a second maximum at around 290 nm, depending on solvent.<sup>24,26–28</sup> Hence, a large portion of the absorption band lies in the UV–B range. An  $n\pi^*$  state has been observed in the circular dichroism (CD) spectra of 2-thiouridine<sup>29</sup> and 2-thiothymidine<sup>30</sup> at about 320 nm, but analogous CD spectra for the nonchiral 2TU cannot be measured. Time-resolved spectroscopy of 2TU was reported in the microsecond regime<sup>27</sup> and the femtosecond regime.<sup>28</sup> For both 2TU and the closely related 2-thiothymine (2TT),<sup>28,30–32</sup> all studies report a near-unity quantum yield for intersystem crossing (ISC) and significant phosphorescence. ISC leads to the formation of long-lived and often very reactive triplet states and is therefore responsible for the loss of photostability. Moreover, in the presence of oxygen,

Received: July 10, 2015

Revised: August 17, 2015

Published: August 18, 2015

reactive oxygen species (e.g., singlet oxygen) can be generated, ultimately leading to DNA damage in a biological environment.

Despite the solid evidence of the high ISC rate of 2TU, the detailed mechanism leading to the population of the harmful triplet states is still not yet understood. Pollum and Crespo-Hernández<sup>28</sup> reported ultrafast (subpicosecond resolution) transient absorption spectra of 2TU and found that the first step after excitation to the  $S_2$  ( $\pi\pi^*$ ) state, which is mainly responsible for the first absorption band, is an ultrafast (<200 fs) internal conversion to the  $S_1$  ( $n\pi^*$ ) state, from where ISC occurs with a time constant of 300–400 fs.

From a theoretical point of view, the topology of the excited-state PES of 2TU was investigated in two recent studies. Cui and Fang<sup>33</sup> reported a large quantity of excited-state minima and crossings, using the multiconfigurational CASPT2//CASSCF methodology (complete active space perturbation theory//complete active space self-consistent field) and imposing planarity ( $C_s$  symmetry) in almost all optimizations. They characterized three (reportedly competing) pathways:  $S_2 \rightarrow S_1 \rightarrow T_1$ ,  $S_2 \rightarrow T_2 \rightarrow T_1$ , and  $S_2 \rightarrow T_3 \rightarrow T_2 \rightarrow T_1$ . However, because it can be expected that most stationary points on the excited-state PES exhibit some degree of out-of-plane distortions, the ISC mechanisms reported by these authors are not reliable. Indeed, Gobbo and Borin<sup>34</sup> (also using CASPT2//CASSCF) found several nonplanar geometries, among them a  $\pi\pi^*$  minimum and a conical intersection between  $\pi\pi^*$  and  $S_0$ . Even though the structural details were different than in the previous study,<sup>33</sup> the latter authors also reported two similar mechanisms,  $S_2 \rightarrow S_1 \rightarrow T_1$  and  $S_2 \rightarrow T_2 \rightarrow T_1$ , as the most likely reaction pathways.

Although ultrafast transient absorption spectroscopy<sup>28</sup> suggests  $S_2 \rightarrow S_1 \rightarrow T_1$  as the most probable pathway, it seems that a complete understanding of the photophysics of 2TU has not been reached yet. A clear identification of the relaxation pathway from theoretical calculations should be obtained by means of dynamical simulations, for example, using the surface hopping nonadiabatic method SHARC<sup>35,36</sup> developed in our group, which allows for a simultaneous description of internal conversion and ISC. As a reference for future excited-state dynamics simulations, in this paper we report a thorough account of all relevant excited-state minima and crossings of 2TU calculated at the highest affordable level of theory, i.e., including electronic correlation by means of CASPT2, not only in the energy calculations but also in the determination of the geometries. This study therefore extends and complements the existing studies of Cui and Fang<sup>33</sup> and Gobbo and Borin,<sup>34</sup> providing the most accurate energies and geometries reported so far. Moreover, the paths connecting the optimized structures were investigated using large-active-space and large-basis-set calculations to assess the viability of smaller active spaces and smaller basis sets for CASPT2-based excited-state dynamics, which will be reported in an upcoming publication.

## ■ THEORETICAL METHODS

**Level of Theory.** Experimental and theoretical studies confirm that 2TU exists in the gas phase and solution only in one tautomeric form, with a thione and a keto group and the prototropic hydrogens attached to the nitrogen atoms.<sup>37–40</sup> Hence, in this study we focus exclusively on this tautomer, whose structure and the numbering of all atoms are given in Figure 1.

To find all structures that might be relevant for the excited-state dynamics of 2TU, geometries were optimized at several levels of theory. First, SA(4 + 3)-CASSCF(14,10)/def2-svp (averaging over 4 singlet and 3 triplet states in a single CASSCF<sup>41</sup>

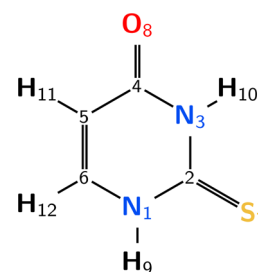


**Figure 1.** Structure of the most stable tautomer of 2TU and atom numbering.

calculation) was employed, using the MOLPRO 2012 suite.<sup>42,43</sup> Second, using COLUMBUS 7,<sup>44,45</sup> we employed MRCIS/cc-pVDZ (multireference configuration interaction including single excitations) with a CAS(6,5) reference space based on SA(4 + 2)-CASSCF(12,9) orbitals. Both methods were used to optimize minima and crossing points between states of the same and of different multiplicity. Third, the minima were additionally optimized using MS(3/3)-CASPT2/cc-pVDZ (multistate CASPT2<sup>46,47</sup> including 3 singlets or 3 triplets) based on SA(4/3)-CASSCF(12,9) orbitals (state-averaging over 4 singlets or 3 triplets in separate CASSCF calculations). These “MS-CASPT2(12,9)” calculations were performed with MOLCAS 8.0,<sup>48,49</sup> the IPEA shift<sup>50</sup> was set to zero and no level shifts were employed. At all levels of theory, the Douglas–Kroll–Hess (DKH) scalar-relativistic Hamiltonian<sup>51</sup> was employed. The composition of the various active and reference spaces is described in the next subsection.

Single-point energies were calculated at the same MRCIS and MS-CASPT2 levels of theory as used for optimizations. Additionally, single-point calculations (at geometries optimized with MS-CASPT2(12,9)) were performed using SA(6/4)-CASPT2, with the default IPEA shift, no level shifts, and the DKH Hamiltonian (the complete procedure is abbreviated as “MS-CASPT2(16,12)” in the following). For these calculations, the atomic Cholesky decomposition<sup>53</sup> method was employed to speed up the calculations. The energies from the MS-CASPT2(16,12) calculations serve as reference for the computationally much more efficient MRCIS/cc-pVDZ and MS-CASPT2(12,9)/cc-pVDZ computations.

State dipole moments were calculated with single-state CASPT2(16,12)/ano-rcc-vqzp, because they are not available at MS-CASPT2 level of theory.

**Orbitals.** Figure 2 shows the orbitals of the largest active space employed in the CAS(16,12) calculations, together with the composition of the reduced active and reference spaces used in this work. In the largest case, the active space contains all the  $\pi$  and  $\pi^*$  orbitals, the  $n_O$  and  $n_S$  lone pairs and the  $\sigma_{CS}$ ,  $\sigma_{CS}^*$  pair. The indices used in the orbital labels refer to the atom(s) where the orbital is (are) mostly localized. The figure is organized such that in the upper row all orbitals corresponding to the acrolein moiety (plus the  $\sigma_{CS}$ ) are listed, whereas the lower row collects the orbitals localized on the thiourea moiety.

At some geometries, it was not possible to obtain a correct CAS(16,12) active space and thus the active space was reduced to CAS(14,11) by excluding the  $n_O$  orbital. The reason for this exclusion is that at the affected geometries, the  $n_O\pi^*$  state is very high in energy and therefore would necessitate a larger number of states in the state-averaging procedure. However, because such a strategy would deteriorate the description of the more relevant lower states, the  $n_O$  orbital was eliminated from the active space.

The  $\sigma_{CS}$ ,  $\sigma_{CS}^*$  pair is not relevant for the description of planar and almost planar geometries, but in the case of  $C_2$

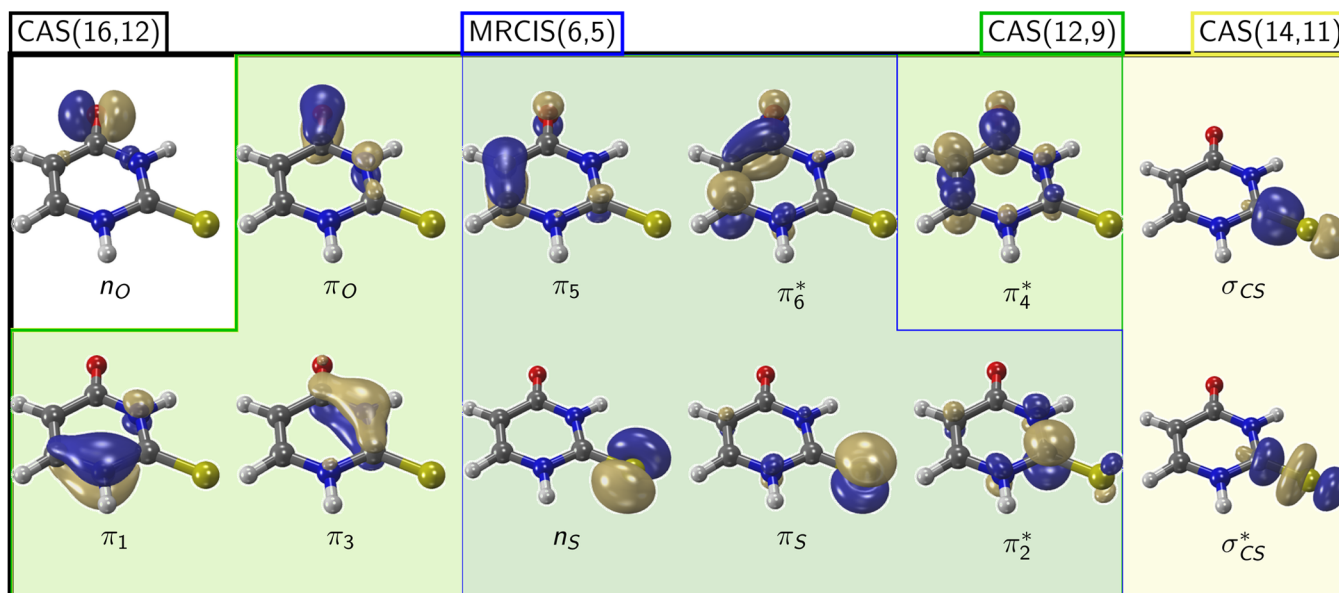


**Figure 2.** Molecular orbitals in the various orbital spaces. The numerical indices of the orbitals refer to the atom where the largest part of the orbital is localized. Except for the  $\sigma$  orbitals on the right, the upper row depicts the acrolein-like orbitals, whereas the lower row depicts the thiourea-like orbitals.

**Table 1.** Vertical Excitation Energies of 2TU in eV (Oscillator Strength in Parentheses), Computed at the MS-CASPT2(12,9)-Optimized Geometry (MRCIS at MRCIS-Optimized Geometry)

state	this work			literature		exp <sup>25,28–30</sup>
	PT2(16,12) <sup>a</sup>	PT2(12,9) <sup>b</sup>	MRCIS(6,5) <sup>c</sup>	Gobbo <sup>34,d</sup>	Cui <sup>33,e</sup>	
$^1n_S\pi_2^*$	3.77 (0.00)	3.70 (0.00)	3.85 (0.00)	3.65 (0.00)	3.83	3.8
$^1\pi_S\pi_6^*$	4.25 (0.35)	4.30 (0.11)	5.78 (0.11)	4.09 (0.24)		4.3
$^1n_O\pi_6^*$	4.65 (0.00)			4.59 (0.00)	4.76	
$^1\pi_S\pi_2^*$	4.72 (0.15)		5.11 (0.39)	4.45 (0.45)	4.46	4.6
$^1n_S\pi_6^*$	5.16 (0.00)	4.89 (0.00)	5.62 (0.00)	4.87 (0.00)		
$^3\pi_S\pi_2^*$	3.51	3.24	3.62	3.14		
$^3n_S\pi_2^*$	3.88	3.76	3.76	3.60		
$^3\pi_S\pi_6^*$	4.11	3.83	4.44	3.67		
$^3n_O\pi_6^*$	4.85		5.62	4.57		

<sup>a</sup>SA(6/4)-CASSCF(16,12) + MS(6/4)-CASPT2/ano-rcc-vqzp, IPEA = 0.25 au. <sup>b</sup>SA(4/3)-CASSCF(12,9) + MS(3/3)-CASPT2/cc-pVDZ, IPEA = 0.0 au. <sup>c</sup>SA(4+2)-CASSCF(12,9) + MRCIS(6,5)/cc-pVDZ. <sup>d</sup>SA(6/6)-CASSCF(14,10) + SS-CASPT2/ano-L-vdzp, IPEA = 0.0 au. <sup>e</sup>SA(4+3)-CASSCF(16,11) + CASPT2/cc-pvdz, IPEA = 0.0 au.

pyramidalization these orbitals mix with the  $\pi$  orbitals and hence should be included in the active space. Yet, and as shown later, a CAS(12,9) active space without the  $\sigma_{CS}$ ,  $\sigma_{CS}^*$  pair leads to a qualitatively correct description of the PESs.

For the MRCIS level of theory, mainly used for the preliminary optimization of crossing points, a reference space CAS(12,9) is still too large and hence was reduced to CAS(6,5), including the  $\pi_S$ ,  $\pi_S$ ,  $n_S$ ,  $\pi_2^*$  and  $\pi_6^*$  orbitals.

## RESULTS AND DISCUSSION

**Vertical Excitation.** Table 1 presents the excited-state energies calculated at the MS-CASPT2-optimized ground-state geometry. In the following, all numbers mentioned in the discussion are from the most accurate MS-CASPT2(16,12)/ano-rcc-vqzp calculations, unless noted otherwise. CASSCF and SS-CASPT2 results are available in the Supporting Information in Table S1.

The ground state of 2TU has a closed-shell configuration. Its calculated dipole moment is 4.29 D (SS-CASPT2), which compares very well with the experimental value of 4.21 D.<sup>54</sup>

The lowest excited singlet state ( $S_1$ ) of 2TU is the  $^1n_S\pi_2^*$  state, where  $\pi_2^*$  is the antibonding  $\pi^*$  orbital located mostly on the C<sub>2</sub> atom. Hence,  $S_1$  describes an excitation that is local to the thiourea moiety of the molecule; the dipole moment of this state is very similar to the ground-state dipole moment (4.29 D at SS-CASPT2). The calculated vertical excitation energy is 3.77 eV (the lower-level calculations in Table 1 agree to within 0.1 eV). With an oscillator strength of approximately zero, this state does not contribute to the UV absorption spectrum. However, in the CD spectra of 2-thiouridine<sup>29</sup> and 2-thiothymidine<sup>30</sup> the  $n_S\pi^*$  state appears at 3.8 eV, which fits very well with the calculated energy.

The  $S_2$  has  $^1\pi_S\pi_6^*$  character and describes an excitation from the  $\pi_S$  orbital, localized on the sulfur atom, to the  $\pi_6^*$  orbital, which is mostly localized on C<sub>6</sub>. As already noted in the literature,<sup>34</sup> this is a charge-transfer state and hence it possesses a large dipole moment, 5.15 D (SS-CASPT2). The energy of the state, 4.25 eV, is in line with the experimental value of 4.3 eV. The calculated oscillator strength is 0.35 and therefore, this state (together with  $^1\pi_S\pi_2^*$ , see below) dominates the low-energy side of the first band of the UV absorption spectrum.

The third excited state ( $S_3$ ) has  ${}^1n_O\pi_6^*$  character; i.e., it corresponds to an excitation from the oxygen lone pair to the  $\pi^*$  orbital mostly localized on  $C_6$ . Unlike  $S_1$  and  $S_2$ , this state cannot be described by the more economic MS-CASPT2(12,9) and MRCIS calculations because they both exclude the  $n_O$  orbital from the active/reference spaces. The energy of this state is 4.65 eV, comparable to the values of Gobbo and Borin<sup>34</sup> and of Cui and Fang.<sup>33</sup> Because the oscillator strength of this state is close to zero, it should not contribute to the absorption spectrum. No experimental data of this state are available. This state shows a comparably small dipole moment of 2.66 D.

The fourth excited state ( $S_4$ ) has  ${}^1\pi_S\pi_2^*$  character and is located at 4.72 eV. Importantly, the values reported in the literature with lower levels of theory<sup>33,34</sup> are underestimated and give rise to a different energetic order, where the  ${}^1\pi_S\pi_2^*$  is below  ${}^1n_O\pi_6^*$  in these studies. This difference is due to the use of the multistate CASPT2 approach in our work, which allows the correct mixing of the states, in contrast to single-state CASPT2. In the MS-CASPT2 calculations, the interaction of  ${}^1\pi_S\pi_2^*$  with the ground state leads to an increase in energy of  ${}^1\pi_S\pi_2^*$ , whereas  ${}^1n_O\pi_6^*$  is down-shifted due to the interaction with  ${}^1n_S\pi_6^*$  ( $S_5$ ), leading to the different state ordering.  ${}^1\pi_S\pi_2^*$  carries a significant oscillator strength (0.15, although 0.26 at SS-CASPT2 level) and together with  ${}^1\pi_S\pi_6^*$  is responsible for the double-peak form of the absorption spectrum, as seen in several solvents.<sup>25,28,29</sup>

The highest computed singlet state ( $S_5$ ) is predicted at 5.16 eV and has  ${}^1n_S\pi_6^*$  character. Again, due to the use of MS-CASPT2 ( ${}^1n_S\pi_6^*$  interacts with  ${}^1n_O\pi_6^*$ , leading to a blue shift of  ${}^1n_S\pi_6^*$ ) this state is higher in energy than in the SS-CASPT2 calculations of Gobbo and Borin.<sup>34</sup> Because the MS-CASPT2(12,9) calculations do not describe the  ${}^1n_O\pi_6^*$  state, no blue-shifting of  ${}^1n_S\pi_6^*$  occurs; consequently, the MS-CASPT2(12,9) value is comparable to the SS-CASPT2 value of Gobbo and Borin.<sup>34</sup>

Table 1 also reports the energies of the lowest triplet states. The lowest triplet state,  $T_1$ , of 2TU is of  ${}^3\pi_S\pi_2^*$  character at the Franck–Condon geometry; its energy is predicted to be 3.51 eV. This energy is slightly higher than the MS-CASPT2(12,9) result and the value reported by Gobbo and Borin.<sup>34</sup> The  $T_2$  state is of  ${}^3n_S\pi_2^*$  character (and hence the triplet counterpart of  $S_1$ ) and is located at 3.88 eV. The third triplet state  $T_3$ , with an energy of 4.11 eV, involves an excitation from a  $\pi$  orbital localized on the  $C_5=C_6$  bond to the antibonding  $\pi_6^*$ . Finally, the last triplet state calculated,  $T_4$ , has an energy of 4.85 eV and, being the counterpart of  $S_3$ , is dominated by  ${}^3n_O\pi_6^*$  character. Unlike with the singlet states, all employed methods predict the same energetic ordering of the lowest triplet states.

Compared to the most accurate MS-CASPT2(16,12) results, the MS-CASPT2(12,9) values and the SS ones given by Gobbo and Borin<sup>34</sup> systematically predict lower excitation energies, especially for the triplet states. This discrepancy can be largely attributed to the different zero-order Hamiltonian (IPEA shift) used in these calculations. Setting the IPEA shift<sup>50</sup> to zero (as in the MS-CASPT2(12,9) calculations and in ref 34) systematically stabilizes open-shell states and hence predicts excitation energies too low. As shown by some authors,<sup>55–57</sup> combining low-quality (double- $\zeta$ ) basis sets with an IPEA shift of zero can lead to significant error compensation, because small basis sets tend to increase the excitation energy, counteracting the effect of neglecting the IPEA shift. Furthermore, the multistate treatment in our MS-CASPT2(16,12) calculations increases most of the excitation energies, because the ground state is stabilized by the interaction with the  ${}^1\pi\pi^*$  states.

Though all the CASPT2 calculations give qualitatively similar results, the MRCIS calculations do not accurately describe the excited states of 2TU, indicating the need of a higher excitation level or a larger reference space. The inclusion of only single excitations is thus not optimal for the excited-state dynamics of 2TU, despite the appealing fact that MRCIS-based dynamics would be much cheaper than CASPT2-based dynamics. One advantage of MRCIS is, though, that it can be used to optimize crossing points including some dynamical correlation (unlike CASSCF), whereas these optimizations are currently not possible with CASPT2.

Notably, the oscillator strength of the  $\pi\pi^*$  states obtained by the different levels of theory differ considerably. Although MRCIS and ref 34 predict the  ${}^1\pi_S\pi_2^*$  state to be the brightest, the MS-CASPT2(16,12) calculations suggest that the lower-energy  ${}^1\pi_S\pi_6^*$  state is brighter (0.35 for  ${}^1\pi_S\pi_6^*$  vs 0.15 for  ${}^1\pi_S\pi_2^*$ ). This behavior is due to the MS-CASPT2 treatment, because at SS-CASPT2 the oscillator strengths are approximately equal (0.25 vs 0.26; Table S1 in the Supporting Information). The oscillator strengths were also computed with EOM-CCSD/cc-pvtz using Molpro<sup>42,43</sup> (results given in Table S1) and it was found that the lower-energy  ${}^1\pi_S\pi_6^*$  state is also brighter (0.39 vs 0.08), in agreement with the MS-CASPT2(16,12) calculation. Intriguingly, the experimental absorption spectra<sup>25,28,29</sup> show two maxima with approximately equal intensity or a band with a shoulder, depending on the solvent. Unfortunately, with the present calculations, it is not possible to distinguish whether the experimental spectrum can be assigned to two states of similar oscillator strengths (and therefore the MS-CASPT2 and EOM-CCSD intensities are incorrect) or due to two states of different oscillator strengths gaining comparable intensity by vibronic effects.

In summary, it was shown that our best MS-CASPT2 vertical excited-state calculations are in excellent agreement with experiment. Smaller-scale MS-CASPT2 calculations, employing smaller basis sets and active spaces, can also describe the lowest excited states reasonably well, although it has to be stressed that this accuracy is partly due to error compensation, where smaller basis sets lead to higher excitation energies, whereas setting the IPEA shift to zero results in lower excitation energies. Furthermore, it has been shown that the inclusion of all relevant orbitals within an MS-CASPT2 calculation is necessary to obtain all excited states and the correct energetic ordering.

In the following, we focus on the relaxation of 2TU after excitation to the lowest bright state,  ${}^1\pi_S\pi_6^*$  ( $S_2$ ). Assuming that the excited states above  $S_2$  do not play a role in the deactivation path, they are not included in the MS-CASPT2(12,9) calculations. In the MS-CASPT2(16,12) calculations, higher states are still included to scrutinize that this assumption is correct (Table S2 in the Supporting Information).

**Excited-State Minima.** Using MS-CASPT2(12,9), minima for the  $S_0$ ,  $S_1$ ,  $S_2$ , and  $T_1$  states have been optimized. In the case of  $S_2$  and  $T_1$ , two different minima have been found in each state, corresponding to the  ${}^1\pi_S\pi_2^*$  and  ${}^1\pi_S\pi_6^*$ , as well as  ${}^3\pi_S\pi_2^*$  and  ${}^3\pi_S\pi_6^*$  characters, hinting at avoided crossings with higher states. The obtained geometries are depicted in Figure 3 and the relevant geometrical parameters are reported in Table 2. To avoid confusion, the columns in the table are labeled according to the wave function character. The energies of all states at all geometries are given in the Supporting Information in Table S2. The optimized geometries are also reported in the Supporting Information.

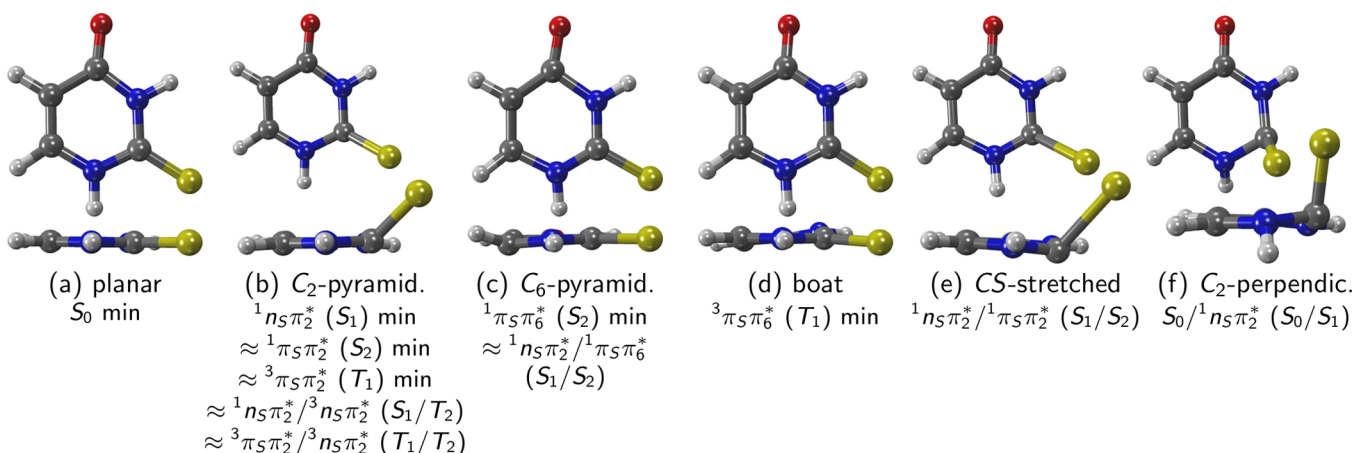


**Figure 3.** Prototypical geometries of the critical points of 2TU. Below the label for each geometry, we list states whose minima/crossings are related to the respective geometry, e.g., the minimum of  ${}^1\pi_5\pi_6^*$  and the  ${}^1n_5\pi_2^*/{}^1\pi_5\pi_6^*$  crossing have geometries similar to (c).

**Table 2.** Geometry Parameters for the Excited-State Minima Optimized at the MS-CASPT2(12,9) Level of Theory<sup>a</sup>

	$S_0$	exc to $\pi_2^*$			exc to $\pi_6^*$	
		$S_1$	$S_2$	$T_1$	$S_2$	$T_1$
$E^b$	0.00	3.45	3.90	3.21	3.93	3.35
$E^c$	0.00	3.33	3.80	2.96	3.75	2.96
$r_{12}$	1.38	1.40	1.38	1.40	<b>1.33</b>	1.37
$r_{23}$	1.38	1.40	1.37	1.41	<b>1.34</b>	1.39
$r_{34}$	1.42	1.41	1.41	1.40	<b>1.51</b>	1.42
$r_{45}$	1.46	1.46	1.46	1.47	<b>1.41</b>	1.45
$r_{56}$	1.36	1.37	1.37	1.38	<b>1.43</b>	<b>1.45</b>
$r_{61}$	1.38	1.37	1.37	1.36	<b>1.43</b>	1.36
$r_{27}$	1.67	<b>1.82</b>	<b>1.93</b>	<b>1.81</b>	<b>1.76</b>	1.71
$r_{48}$	1.22	1.23	1.22	1.23	1.24	1.23
$a_{127}$	122.5	<b>117.4</b>	<b>110.6</b>	<b>110.7</b>	120.3	120.7
$a_{348}$	120.3	120.3	120.8	121.3	<b>114.8</b>	120.0
$p_{7213}$	-0.1	<b>39.1</b>	<b>47.3</b>	<b>44.5</b>	-1.9	3.0
$p_{8435}$	0.0	-1.7	0.0	1.1	1.1	0.5
$p_{10324}$	1.1	-0.8	-0.4	-8.5	5.7	<b>-20.5</b>
$p_{12651}$	0.1	-0.6	-0.2	-0.5	<b>26.5</b>	-5.4
Q	0.01	<b>0.04</b>	<b>0.04</b>	<b>0.10</b>	<b>0.08</b>	<b>0.16</b>
B	planar	$E_2$	$E_2$	$E_2$	$E_6$	$B_{3,6}$

<sup>a</sup>Important parameters are marked in bold. Q is the puckering amplitude;<sup>58</sup> B is the Boeyens<sup>59</sup> symbol for six-membered rings. Energies are in eV,  $r$  and Q in Å, and angles  $a$  and pyramidalization angles  $p$  (defined in the Supporting Information) in degrees. States are labeled according to energetic order ( $S_0$ ,  $S_1$ , ...) and wavefunction character. <sup>b</sup>MS(6/4)-CASPT2(16,12)/ano-rcc-vqzp, IPEA = 0.25 au. <sup>c</sup>MS(4/3)-CASPT2(12,9)/cc-pvdz, IPEA = 0.0 au.

We note here that all energies mentioned in the following are from the MS-CASPT2(16,12)/ano-rcc-vqzp calculations, with the MS-CASPT2(12,9)/cc-pvdz energies given in parentheses.

The ground-state geometry (Figure 3a) is nearly planar. The lengths of the C–N bonds ( $r_{12}$ ,  $r_{23}$ ,  $r_{34}$ ,  $r_{61}$ , recall Figure 1) are approximately equal, with values from 1.38 to 1.42 Å. The C–C bonds have  $r_{45} = 1.46$  Å (single bond) and  $r_{56} = 1.36$  Å (double bond). These and all other bond lengths compare reasonably well to the best-estimate values of ref 40, but our bonds are systematically too long due to the use of a double- $\zeta$  basis set in the optimizations.

Compared to the ground-state minimum, the minimum of the  ${}^1n_5\pi_2^*$  ( $S_1$  state) shows no major differences in the bond

lengths, except for the  $C_2=S$  bond, which is much longer than for  $S_0$ . The most important geometrical feature of this minimum is the strong pyramidalization at  $C_2$ , leading to the sulfur atom being strongly displaced out of the molecular plane (Figure 3b). Although the ring itself is still almost planar, a slight puckering of the  $C_2$  atom away from the sulfur atom is noticeable ( $E_2$  in Boeyens notation<sup>59</sup>). The  $S_1$  energy at its minimum is 3.45 eV (3.33 eV).

The minima of  ${}^1\pi_5\pi_2^*$  ( $S_2$ ) and  ${}^3\pi_5\pi_2^*$  ( $T_1$ ) are structurally very similar to the  ${}^1n_5\pi_2^*$  minimum (also Figure 3b), because in all these states the  $\pi_2^*$  orbital is populated. These minima also feature a mostly planar ring with bond lengths and angles similar to the those of the ground state, a slight puckering and strong pyramidalization at  $C_2$  and a strongly enlarged  $C_2=S$  bond. However, the  ${}^1\pi_5\pi_2^*$  and  ${}^3\pi_5\pi_2^*$  structures show an even larger pyramidalization angle  $p_{7213}$  than the  ${}^1n_5\pi_2^*$  minimum. The energies of the  ${}^1n_5\pi_2^*$ ,  ${}^1\pi_5\pi_2^*$ , and  ${}^3\pi_5\pi_2^*$  minima are fairly low (Table 2), and from comparison with the energies of the other minima, it is apparent that  $C_2$  pyramidalization is a highly probable process in the deactivation. Surprisingly, however, no  $C_2$ -pyramidalized geometries were reported in the literature.<sup>27,33,34</sup> For completeness, we checked the existence of the  $C_2$ -pyramidalized minima for  $T_1$  and  $S_1$  with MRCIS as well as the methods used in ref 34 (SA(6/6)-CASSCF(14,10)/ANO-L- $v$ dzp) and ref 27 (UB3LYP/aug-cc-pvdz, only  $T_1$ ) and found in all cases that the optimizations yielded pyramidalized geometries. One can thus safely assume that  $C_2$ -pyramidalized minima exist in 2TU, analogous to the ones reported for the related compounds 6-aza-2-thiothymine<sup>60</sup> ( ${}^1n\pi^*$ ,  ${}^3n\pi^*$ ) and thiourea<sup>61</sup> ( ${}^3n\pi^*$ ).

We also identified a second minimum on the  $S_2$  adiabatic potential energy surface, where the wave function character is  ${}^1\pi_5\pi_6^*$ . This geometry (Figure 3c) features bond inversion (i.e., short bonds become longer and long ones shorter, compared to the ground state) in the ring, an elongated  $C_2=S$  bond, and puckering and quite notable pyramidalization on  $C_6$ , due to a weakening of the  $C=S$  bond and the increased electron density at  $C_6$ . The  $S_2$  energy at this minimum is 3.93 eV (3.75 eV).

The counterpart on the  $T_1$  potential (Figure 3d) with  ${}^3\pi_5\pi_6^*$  character also shows an elongated  $C_5=C_6$  bond, no bond inversion but pyramidalization at  $N_3$ , and a slight, boat-like distortion of the ring. The  $T_1$  energy at this minimum is 3.35 eV (2.96 eV).

**Excited-State Crossing Points.** Due to limitations in the existing implementations of the CASPT2 method, it was not

possible to optimize crossing points at this level of theory. Instead, crossing points were optimized at CASSCF(14,10)/def2-svp and MRCIS(6,5)/cc-pvdz levels of theory. Because these geometries are not necessarily points of degeneracy at the more accurate CASPT2 level of theory, the crossing geometries were refined with the help of linear interpolation in internal coordinates (LIIC) scans between the CASSCF or MRCIS crossing points and the corresponding CASPT2 minima. Single-point calculations along the LIIC paths were carried out at the MS-CASPT2(12,9)/cc-pVDZ level to locate the geometry with the smallest energy gap between the relevant states. Only at the latter geometries, constituting the best estimate of the crossing point at MS-CASPT2(12,9) level, were the MS-CASPT2(16,12) reference single point calculations performed. Note that we discuss only the MS-CASPT2-refined geometries in the following, but not the geometries optimized at the CASSCF or MRCIS level of theory. The refined geometries are reported in the [Supporting Information](#).

We report first a conical intersection between the  $^1n_s\pi_2^*$  and  $^1\pi_s\pi_6^*$  ( $S_1/S_2$ ) states. Because this structure is located close to the  $^1\pi_s\pi_6^*$  minimum, it has a very similar geometry, yet featuring a slightly more pronounced pyramidalization at  $C_6$  (recall [Figure 3c](#)). The geometry was obtained from a LIIC scan between the MS-CASPT2-optimized  $^1\pi_s\pi_6^*$  minimum and the CASSCF(14,10)-optimized  $^1\pi_s\pi_6^*/^1n_s\pi_2^*$  crossing point. At the MS-CASPT2(12,9) level of theory, the energies of  $S_1/S_2$  are 3.79/3.79 eV, which is only 0.04 eV above the  $^1\pi_s\pi_6^*$  minimum. Hence, it could be expected that the system very quickly relaxes to  $S_1$  after reaching the  $S_2$  ( $^1\pi_s\pi_6^*$ ) minimum. One should note that the crossing is slightly moved at the more accurate MS-CASPT2(16,12) level of theory, according to the corresponding  $S_1/S_2$  energies (3.73/3.92 eV).

Another conical intersection between  $^1n_s\pi_2^*$  and  $^1\pi_s\pi_2^*$  ( $S_1/S_2$ ) was located on the LIIC between the conical intersection optimized at MRCIS(6,5) level and the MS-CASPT2-optimized  $^1n_s\pi_2^*$  minimum. The geometry is similar to the ones of the  $^1n_s\pi_2^*$  and  $^1\pi_s\pi_2^*$  minima, featuring strong  $C_2$  pyramidalization. However, it is distinguished by a C=S bond length of about 2.3 Å ([Figure 3e](#)); at this bond length, the  $n_s$  and  $\pi_s$  orbitals become approximately degenerate, leading to a degeneracy of the  $^1n_s\pi_2^*$  and  $^1\pi_s\pi_2^*$  states. The energies of the involved states are 4.24/4.29 eV (4.07/4.08 eV), making this crossing much less accessible than the previous one. It might, however, be a relaxation pathway for molecules otherwise trapped in the  $S_2$  ( $^1\pi_s\pi_2^*$ ) minimum.

A conical intersection connecting the  $^1n_s\pi_2^*$  ( $S_1$ ) with the ground state is depicted in [Figure 3f](#). It was optimized at MRCIS level and shows  $C_2$  pyramidalization, but with an even larger pyramidalization angle  $p_{7213}$  of about  $56^\circ$  ( $\alpha_{127}$  is  $90^\circ$ ), and also strong pyramidalization at  $N_1$ . It appears that  $C_2$  pyramidalization destabilizes the  $S_0$  much more than the  $S_1$ , which leads to the crossing. This type of perpendicular pyramidalization is also known from other systems, e.g., 6-thioguanine<sup>18</sup> or uracil.<sup>62</sup> The energies of this  $S_0/S_1$  crossing are 3.39/3.93 eV (3.56/3.85 eV), showing a significant energy gap between the involved states. However, given the energy of the  $^1n_s\pi_2^*$  minimum (3.47 eV at MS-CASPT2(16,12), or 3.33 eV at MS-CASPT2(12,9)), this crossing is not expected to be an important relaxation pathway, in agreement with the experimental observation of near-unity ISC yields.<sup>28,31,63</sup> In passing, we note that we were not able to reproduce the ethylenic  $S_0/S_1$  conical intersection described by Gobbo and Borin.<sup>34</sup>

A minimum energy crossing point between  $S_1$  and  $T_2$  ( $^3n_s\pi_2^*$ ) was found from a LIIC connecting the  $^1n_s\pi_2^*$  minimum and the

$S_1/T_2$  crossing optimized at MRCIS level of theory. The energies of  $S_1/T_2$  are 3.51/3.60 eV (3.42/3.33 eV), which is less than 0.1 eV above the  $S_1$  minimum energy. The existence of this singlet–triplet crossing in direct vicinity of the  $S_1$  minimum (the geometry is also of  $C_2$ -pyramidalized type as in [Figure 3b](#) and only slightly different from the  $S_1$  minimum geometry) is crucial to the very efficient ISC channel in 2TU. At the crossing geometry, the SOC between the involved states is about  $130\text{ cm}^{-1}$ , in apparent contradiction to El-Sayed's rule,<sup>64</sup> because both states are of  $n_s\pi_2^*$  character. However, due to strong nonplanarity, the states involved are not strictly  $n_s\pi_2^*$ , enhancing spin–orbit coupling.

The last crossing found is a conical intersection between  $^3\pi_s\pi_2^*$  and  $^3n_s\pi_2^*$  ( $T_1/T_2$ ), which was obtained from a LIIC scan between the MRCIS-optimized  $T_1/T_2$  crossing and the  $S_1$  minimum. This crossing is located at 3.31/3.39 eV (3.21/3.26 eV), slightly below the singlet–triplet crossing described above. Also this geometry is of the  $C_2$ -pyramidalized type ([Figure 3b](#)). This crossing allows for ultrafast internal conversion from  $^3n_s\pi_2^*$  to  $^3\pi_s\pi_2^*$  and subsequent relaxation to the  $^3\pi_s\pi_2^*$  minimum. The efficient relaxation to  $^3\pi_s\pi_2^*$  and the resulting very small  $^3n_s\pi_2^*$  population is likely the reason that Pollum and Crespo-Hernández<sup>28</sup> did not find any evidence of the  $^3n_s\pi_2^*$  state.

**Reaction Paths.** To establish the photodeactivation reaction paths, additional LIIC scans have been carried out to connect the minima and the calculated crossing points. Three chains of LIICs have been constructed:  $S_0 \rightarrow ^1\pi_s\pi_2^* \rightarrow ^1n_s\pi_2^*/^1\pi_s\pi_6^* \rightarrow ^1n_s\pi_2^*$  (Path I);  $S_0 \rightarrow ^1\pi_s\pi_6^* \rightarrow ^1n_s\pi_2^*/^1\pi_s\pi_6^* \rightarrow ^1n_s\pi_2^*$  (Path II), both ending at the  $S_1$  minimum; and  $^1n_s\pi_2^* \rightarrow ^1n_s\pi_2^*/^3n_s\pi_2^* \rightarrow ^3\pi_s\pi_2^*/^3n_s\pi_2^* \rightarrow ^3\pi_s\pi_2^* \rightarrow ^3\pi_s\pi_6^*$  (Path III), which leads from the  $S_1$  minimum to the  $T_1$  minima and hence is the continuation of both Paths I and II. All 59 geometries from the LIIC chains are given in the [Supporting Information](#). The three LIIC chains are depicted side-by-side in [Figure 4](#), together with the assumed relaxation pathway.

The calculations were performed with MS-CASPT2(12,9)/cc-pVDZ and with MS(4/3)-CASPT2(14,11)/ano-rcc-vtzp (with the default IPEA shift). Only the smaller CAS(14,11) active space was used because for  $C_2$ -pyramidalized geometries the  $1n_o\sigma^*$  states are very high in energy and hence the  $n_o$  orbital could not be kept in the active space along the complete path. For both methods, an imaginary level shift<sup>65</sup> of 0.2 au was used to avoid intruder states and to obtain smooth potentials. [Figure S2](#) in the [Supporting Information](#) presents the same LIIC paths using single-state CASPT2, showing almost quantitative agreement of SS- and MS-CASPT2. Hence, we are confident that our MS-CASPT2 calculations provide a correct description of the relaxation pathways, without suffering from the possible artifacts of MS-CASPT2 calculations as discussed by Serrano-Andrés et al.<sup>66</sup>

Due to the presence of two competing minima on the  $S_2$  PES—the  $^1\pi_s\pi_2^*$  and  $^1\pi_s\pi_6^*$  minima—there are two possible relaxation routes (Paths I and II) leading the system away from the Franck–Condon region. Based on static calculations alone, it is not possible to know which  $S_2$  minimum is reached after excitation; dynamics simulations are necessary to clarify this issue. However, considering that Path I necessitates the motion of the heavy sulfur atom, it is conceivable that the system will initially follow Path II.

Path II is much more efficient for  $S_2 \rightarrow S_1$  internal conversion than Path I. With respect to the  $^1\pi_s\pi_6^*$  minimum (Path II), the neighboring  $S_1/S_2$  conical intersection ( $^1n_s\pi_2^*/^1\pi_s\pi_6^*$ ) is less than 0.1 eV higher in energy, and structurally very similar.

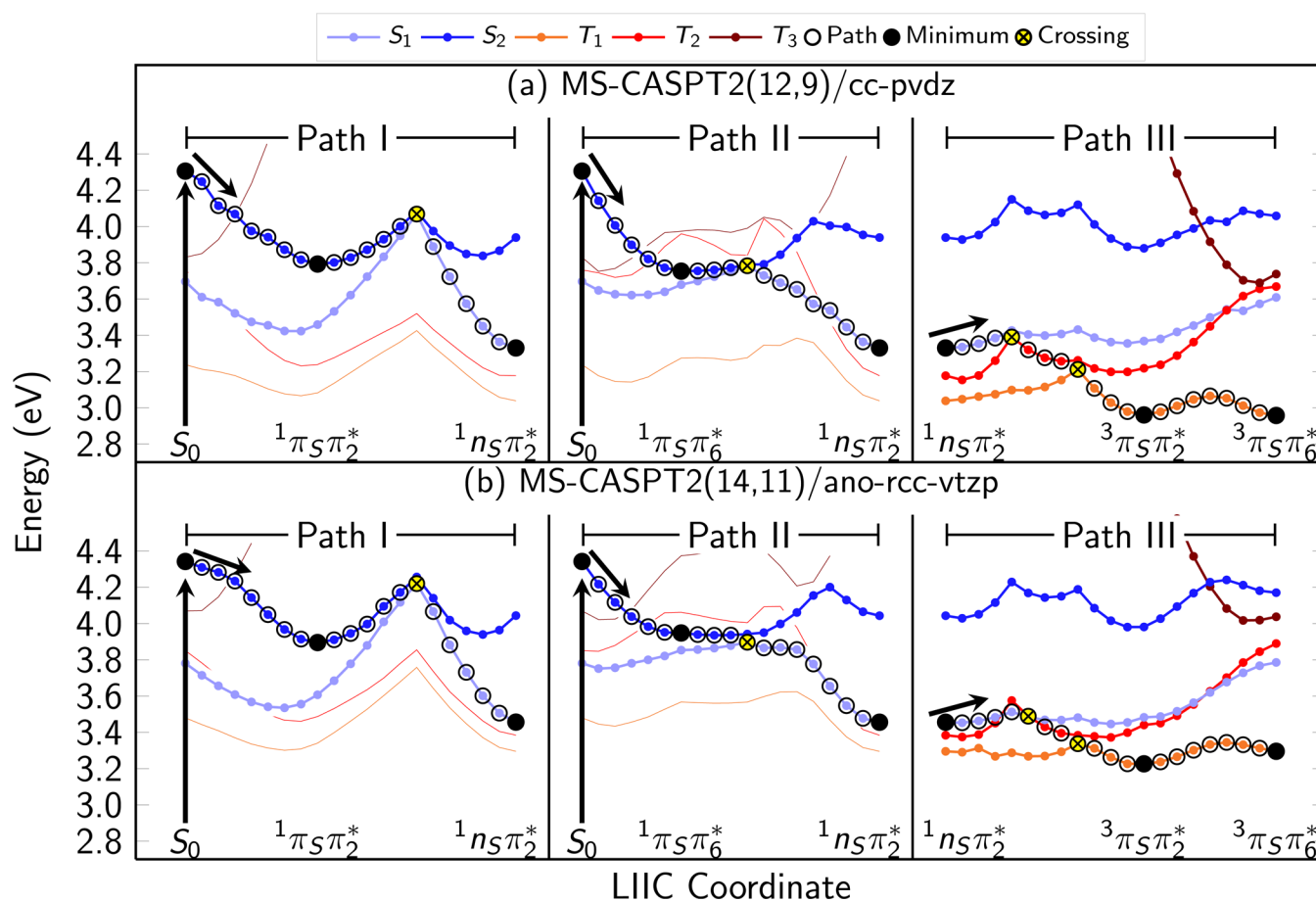


**Figure 4.** LIIC paths along the critical points of 2-thiouracil. The upper panel (a) shows the MS-CASPT2(12,9)/cc-pvdz energies; the lower panel (b) shows the reference energies from MS-CASPT2(14,11)/ano-rcc-vtzp. Open black circles mark the proposed relaxation pathway, full black circles mark minima discussed in the text, and crosses mark crossing points. The character of the optimized states are given below the fill circles. The black arrows mark the vertical excitation from the ground-state minimum.

Conversely, from the  $^1\pi_S\pi_2^*$  minimum (Path I) a barrier of about 0.3 eV needs to be surmounted to reach the  $S_1/S_2$  crossing point ( $^1n_S\pi_2^*/^1\pi_S\pi_2^*$ ). A slightly smaller barrier separates the two  $S_2$  minima; hence it could be possible that trajectories initially following Path I eventually relax through Path II. ISC should not be able to compete with IC at this point in the dynamics because along Path I no triplet states are close in energy to the  $S_2$  minimum and relaxation through Path II is expected to be exceptionally fast.

Both Path I and Path II coalesce at the  $S_1$  ( $^1n_S\pi_2^*$ ) minimum, from where Path III leads to the  $T_1$  minima. The  $S_1$  PES around the minimum is quite flat and only a very small barrier of 0.05 eV (0.09 eV) needs to be overcome to reach a crossing point with the  $T_2$ . Because the system should be trapped in the  $S_1$  state (the  $S_0/S_1$  conical intersection is about 0.5 eV above the  $S_1$  minimum), it is very likely that 2TU will eventually undergo intersystem crossing to the  $T_2$  state. The large SOC and the small energy gap between  $S_1$  and  $T_2$  support the experimentally observed ISC time scale of 300–400 fs.<sup>28</sup>

As can be seen in the LIIC scans, from the  $S_1/T_2$  crossing a barrierless path is available to reach the  $T_1/T_2$  conical intersection and to immediately decay to  $T_1$ , followed by relaxation to the  $T_1$  ( $^3\pi_S\pi_2^*$ ) minimum. Because both the  $T_1/T_2$  crossing point and the  $^3\pi_S\pi_2^*$  minimum also show  $C_2$  pyramidalization, no large atomic motion is necessary to accomplish decay to  $T_1$ .

However, besides the  $^3\pi_S\pi_2^*$  ( $T_1$ ) minimum, a second  $T_1$  minimum with  $^3\pi_S\pi_6^*$  character and a very similar energy exists.

Only a small barrier of about 0.12 eV (0.10 eV) separates the two minima, so that it can be expected that the system will equilibrate between them. Based on quantum chemistry alone, it is not possible to judge how the system will relax to these two minima. The calculated energies of the  $^3\pi_S\pi_6^*$  and  $^3\pi_S\pi_2^*$  minima are 3.35 and 3.21 eV (2.96 and 2.96 eV) and hence both fit quite well with the value of 3.17 eV of the zero-zero emission of phosphorescence reported by Taherian et al.<sup>31</sup> However, the large peak at the zero-zero emission<sup>31</sup> of the phosphorescence spectrum might indicate that the geometries of the  $S_0$  and the emitting triplet state are not very different, which could be a hint that the emitting triplet is  $^3\pi_S\pi_6^*$ . On the contrary, the same authors<sup>31</sup> concluded that the  $T_1$  minimum is likely to be non-planar on the basis of the polarization of the phosphorescence emission. Clearly, dynamical simulations are needed to clarify the relative importance of the two  $T_1$  minima.

From the computational point of view, it is important to note that the MS-CASPT2(12,9)/cc-pvdz level of theory can reproduce all important features of the excited-state PES, compared to MS-CASPT2(14,11)/ano-rcc-vtzp (Figure 4). Especially the singlet potentials are very similar, whereas the triplet states show slightly larger deviations. For example, around the  $^1\pi_S\pi_2^*$  minimum the  $T_2$  and  $T_3$  states are above the  $S_2$  at the MS-CASPT2(14,11) level, whereas they are close to each other at MS-CASPT2(12,9) level. Furthermore, MS-CASPT2(12,9) seems to overstabilize the  $T_1$  minima in comparison with the

other states, which might be a case where the errors of basis set effect and IPEA shift do not cancel out as it is the case around the Franck–Condon region. In summary, the deviations between MS-CASPT2(12,9) and the larger calculations are acceptable, considering that a MS-CASPT2(12,9)/cc-pvdz single point calculation is about 10 times faster than MS-CASPT2(14,11)/ano-rcc-vtzp and almost 100 times faster than MS-CASPT2(16,12)/ano-rcc-vqzp. One should stress, however, that this close agreement is only due to error compensation in the small calculation, where the increase in excitation energy due to a small basis set (like cc-pvdz) is canceled to a large degree by the effect of setting the IPEA shift to zero. This error compensation is in line with others reported in the literature.<sup>55–57</sup>

In summary, we then conclude that our calculations indicate  $S_2 \rightarrow S_1 \rightarrow T_2 \rightarrow T_1$  to be the primary relaxation pathway for 2TU. We expect direct  $S_2 \rightarrow S_1 \rightarrow T_1$  ISC to be only a side channel, because around the  $S_1$  minimum the  $S_1$ – $T_1$  energy gap is always larger than the  $S_1$ – $T_2$  gap and the  $S_1$ – $T_1$  SOC is smaller than the  $S_1$ – $T_2$  SOC (50 and 150  $\text{cm}^{-1}$ , respectively). This conclusion is contrary to the findings of Cui and Fang<sup>33</sup> and Gobbo and Borin,<sup>34</sup> who reported that direct  $S_2 \rightarrow S_1 \rightarrow T_1$  ISC should occur. The finding that ISC involves the  $T_2$  is not considered by Pollum and Crespo-Hernández,<sup>28</sup> who reported  $S_2 \rightarrow S_1 \rightarrow T_1$  on the basis of transient absorption spectroscopy. However, the presence of the  $T_1/T_2$  conical intersection and the small energetic gap between those states allow for ultrafast internal conversion from  $T_2$  to  $T_1$ , with a very low transient  $T_2$  population which thus might be hard to observe.

## CONCLUSIONS

A comprehensive study of the excited-state potential energy surfaces of 2-thiouracil has been reported, employing accurate multireference quantum chemical methods up to MS-CASPT2(16,12), basis sets of up to quadruple- $\zeta$  quality and geometries optimized at MS-CASPT2 level. The results show that the lowest  $S_1$  minimum is strongly pyramidalized at  $C_2$  and that two relaxation paths allow to reach this minimum from the Franck–Condon region. From the  $S_1$  minimum, the  $T_2$  triplet state can be accessed nearly barrierlessly, and substantial spin–orbit couplings are likely to lead to efficient, subpicosecond ISC. Subsequent relaxation from  $T_2$  to  $T_1$  is barrierless. The relaxation is expected to ultimately lead to one of two  $T_1$  minima, one with a slight boat-like conformation of the pyrimidine ring, the other with  $C_2$  pyramidalization. In summary, the photochemical reaction sequence is  $S_2 \rightarrow S_1 \rightarrow T_2 \rightarrow T_1$ .

As a methodological note, the results from MS-CASPT2(16,12)/ano-rcc-vqzp are compared to MS-CASPT2(12,9)/cc-pvdz, where in the latter calculations the IPEA shift<sup>50</sup> was set to zero. The two methods show a very good agreement, all relevant parts of the PES are accurately reproduced by the computationally much more efficient MS-CASPT2(12,9) method. One can therefore conclude that nonadiabatic dynamics simulations at this level of theory should produce an accurate picture of the deactivation of 2TU. Work along these lines is planned for the future.

## ASSOCIATED CONTENT

### Supporting Information

The Supporting Information is available free of charge on the ACS Publications website at DOI: 10.1021/acs.jpca.5b06639.

Definition of pyramidalization angles. Vertical excitation energies, dipole moments, and oscillator strength at

CASSCF, SS-CASPT2, MS-CASPT2, and EOM-CCSD levels of theory. Relative energies of all states ( $S_1$  to  $S_3$ ,  $T_1$  to  $T_3$ ) at all critical points. SS-CASPT2 LIIC paths. XYZ coordinates of all critical points and all coordinates used in Figure 4. References 43, 45, 48, and 49 are provided in complete form as part of the references cited in the Supporting Information. (PDF)

## AUTHOR INFORMATION

### Corresponding Authors

\*P. Marquetand. E-mail: philipp.marquetand@univie.ac.at.

\*L. González. E-mail: leticia.gonzalez@univie.ac.at.

### Notes

The authors declare no competing financial interest.

## ACKNOWLEDGMENTS

The authors acknowledge support from the Austrian Science Fund (FWF) through project P25827, as well as the COST actions CM1204 (XLIC) and CM1305 (ECOSTBio). Part of the calculations have been carried out with the help of the Vienna Scientific Cluster (VSC). Antonio Borin is warmly thanked for providing initial geometries and for fruitful discussions. The authors also want to thank Susanne Ullrich, Carlos Crespo-Hernández, and Inés Corral for related scientific discussions.

## REFERENCES

- (1) Périgaud, C.; Gosselin, G.; Imbach, J. L. Nucleoside Analogues as Chemotherapeutic Agents: A Review. *Nucleosides Nucleotides* **1992**, *11*, 903–945.
- (2) Favre, A.; Saintomé, C.; Fourrey, J.-L.; Clivio, P.; Laugãa, P. Thionucleobases as intrinsic photoaffinity probes of nucleic acid structure and nucleic acid-protein interactions. *J. Photochem. Photobiol., B* **1998**, *42*, 109–124.
- (3) Wilhelmsson, L. M. Fluorescent nucleic acid base analogues. *Q. Rev. Biophys.* **2010**, *43*, 159–183.
- (4) Sinkeldam, R. W.; Greco, N. J.; Tor, Y. Fluorescent Analogs of Biomolecular Building Blocks: Design, Properties, and Applications. *Chem. Rev.* **2010**, *110*, 2579–2619.
- (5) Crespo-Hernández, C. E.; Cohen, B.; Hare, P. M.; Kohler, B. Ultrafast Excited-State Dynamics in Nucleic Acids. *Chem. Rev.* **2004**, *104*, 1977–2020.
- (6) Middleton, C. T.; de La Harpe, K.; Su, C.; Law, Y. K.; Crespo-Hernández, C. E.; Kohler, B. DNA Excited-State Dynamics: From Single Bases to the Double Helix. *Annu. Rev. Phys. Chem.* **2009**, *60*, 217–239.
- (7) Barbatti, M.; Borin, A. C.; Ullrich, S., Eds. *Photoinduced Phenomena in Nucleic Acids*; Topics in Current Chemistry; Springer: Berlin Heidelberg, 2015.
- (8) Pollum, M.; Martínez-Fernández, L.; Crespo-Hernández, C. E. In *Photoinduced Phenomena in Nucleic Acids I*; Barbatti, M., Borin, A. C., Ullrich, S., Eds.; Topics in Current Chemistry; Springer: Berlin Heidelberg, 2014; Vol. 356, pp 245–327.
- (9) Matsika, S. *Photoinduced Phenomena in Nucleic Acids I*; Topics in Current Chemistry; Springer: Berlin Heidelberg, 2014; Vol. 355, pp 209–243.
- (10) Crespo-Hernández, C. E.; Martínez-Fernández, L.; Rauer, C.; Reichardt, C.; Mai, S.; Pollum, M.; Marquetand, P.; González, L.; Corral, I. Electronic and Structural Elements That Regulate the Excited-State Dynamics in Purine Nucleobase Derivatives. *J. Am. Chem. Soc.* **2015**, *137*, 4368–4381.
- (11) Pollum, M.; Jockusch, S.; Crespo-Hernández, C. E. 2,4-Dithiothymine as a Potent UVA Chemotherapeutic Agent. *J. Am. Chem. Soc.* **2014**, *136*, 17930–17933.
- (12) Ajitkumar, P.; Cherayil, J. D. Thionucleosides in transfer ribonucleic acid: diversity, structure, biosynthesis, and function. *Microbiol. Rev.* **1988**, *52*, 103.

- (13) WHO Model Lists of Essential Medicines. available from <http://www.who.int/medicines/publications/essentialmedicines/en/> (accessed July 5, 2015).
- (14) Euvrard, S.; Kanitakis, J.; Claudy, A. Skin Cancers after Organ Transplantation. *N. Engl. J. Med.* **2003**, *348*, 1681–1691.
- (15) Attard, N. R.; Karran, P. UVA photosensitization of thiopurines and skin cancer in organ transplant recipients. *Photochem. Photobiol. Sci.* **2012**, *11*, 62–68.
- (16) Karran, P.; Attard, N. Thiopurines in current medical practice: molecular mechanisms and contributions to therapy-related cancer. *Nat. Rev. Cancer* **2008**, *8*, 24.
- (17) Reichardt, C.; Guo, C.; Crespo-Hernández, C. E. Excited-State Dynamics in 6-Thioguanosine from the Femtosecond to Microsecond Time Scale. *J. Phys. Chem. B* **2011**, *115*, 3263–3270.
- (18) Martínez-Fernández, L.; González, L.; Corral, I. An Ab Initio Mechanism for Efficient Population of Triplet States in Cytotoxic Sulfur Substituted DNA Bases: The Case of 6-Thioguanine. *Chem. Commun.* **2012**, *48*, 2134–2136.
- (19) Martínez-Fernández, L.; Corral, I.; Granucci, G.; Persico, M. Competing Ultrafast Intersystem Crossing and Internal Conversion: a Time Resolved Picture for the Deactivation of 6-Thioguanine. *Chem. Sci.* **2014**, *5*, 1336.
- (20) Cooper, D. S. Antithyroid Drugs. *N. Engl. J. Med.* **2005**, *352*, 905–917.
- (21) Wätjen, F.; Buchardt, O.; Langvad, E. Affinity therapeutics. 1. Selective incorporation of 2-thiouracil derivatives in murine melanomas. Cytostatic activity of 2-thiouracil arotinoids, 2-thiouracil retinoids, arotinoids, and retinoids. *J. Med. Chem.* **1982**, *25*, 956–960.
- (22) Basinger, M. A.; Casas, J.; Jones, M. M.; Weaver, A. D.; Weinstein, N. H. Structural requirements for Hg(II) antidotes. *J. Inorg. Nucl. Chem.* **1981**, *43*, 1419–1425.
- (23) Kameda, K.; Iwamoto, S.; Kominami, S.; Ohnishi, T. Induction of Cell Killing, Mutation and umu Gene Expression by 6-Mercaptopurine or 2-Thiouracil with UVA Irradiation. *Photochem. Photobiol.* **1997**, *65*, 115–118.
- (24) Párkányi, C.; Boniface, C.; Aaron, J.-J.; Gaye, M. D.; Ghosh, R.; von Szentpály, L.; Raghuveer, K. S. Electronic absorption and fluorescence spectra and excited singlet-state dipole moments of biologically important pyrimidines. *Struct. Chem.* **1992**, *3*, 277–289.
- (25) Khvorostov, A.; Lapinski, L.; Rostkowska, H.; Nowak, M. J. UV-Induced Generation of Rare Tautomers of 2-Thiouracils: A Matrix Isolation Study. *J. Phys. Chem. A* **2005**, *109*, 7700–7707.
- (26) Moustafa, H.; Shibl, M. F.; Hilal, R. Electronic Absorption Spectra of Some 2-Thiouracil Derivatives. *Phosphorus, Sulfur Silicon Relat. Elem.* **2005**, *180*, 459–478.
- (27) Vendrell-Criado, V.; Saez, J. A.; Lhiaubet-Vallet, V.; Cuquerella, M. C.; Miranda, M. A. Photophysical properties of 5-substituted 2-thiopyrimidines. *Photochem. Photobiol. Sci.* **2013**, *12*, 1460–1465.
- (28) Pollum, M.; Crespo-Hernández, C. E. Communication: The dark singlet state as a doorway state in the ultrafast and efficient intersystem crossing dynamics in 2-thiothymine and 2-thiouracil. *J. Chem. Phys.* **2014**, *140*, 071101.
- (29) Igarashi-Yamamoto, N.; Tajiri, A.; Hatano, M.; Shibuya, S.; Ueda, T. Ultraviolet absorption, circular dichroism and magnetic circular dichroism studies of sulfur-containing nucleic acid bases and their nucleosides. *Biochim. Biophys. Acta, Nucleic Acids Protein Synth.* **1981**, *656*, 1–15.
- (30) Taras-Goślińska, K.; Burdziński, G.; Wenska, G. Relaxation of the T<sub>1</sub> excited state of 2-thiothymine, its riboside and deoxyriboside-enhanced nonradiative decay rate induced by sugar substituent. *J. Photochem. Photobiol., A* **2014**, *275*, 89–95.
- (31) Taherian, M.-R.; Maki, A. Optically detected magnetic resonance study of the phosphorescent states of thiouracils. *Chem. Phys.* **1981**, *55*, 85–96.
- (32) Kuramochi, H.; Kobayashi, T.; Suzuki, T.; Ichimura, T. Excited-State Dynamics of 6-Aza-2-thiothymine and 2-Thiothymine: Highly Efficient Intersystem Crossing and Singlet Oxygen Photosensitization. *J. Phys. Chem. B* **2010**, *114*, 8782–8789.
- (33) Cui, G.; Fang, W.-h. State-specific heavy-atom effect on intersystem crossing processes in 2-thiothymine: A potential photo-dynamic therapy photosensitizer. *J. Chem. Phys.* **2013**, *138*, 044315.
- (34) Gobbo, J. P.; Borin, A. C. 2-Thiouracil deactivation pathways and triplet states population. *Comput. Theor. Chem.* **2014**, *1040–1041*, 195–201.
- (35) Richter, M.; Marquetand, P.; González-Vázquez, J.; Sola, I.; González, L. SHARC: ab Initio Molecular Dynamics with Surface Hopping in the Adiabatic Representation Including Arbitrary Couplings. *J. Chem. Theory Comput.* **2011**, *7*, 1253–1258.
- (36) Mai, S.; Marquetand, P.; González, L. A general method to describe intersystem crossing dynamics in trajectory surface hopping. *Int. J. Quantum Chem.* **2015**, *115*, 1215.
- (37) Les, A.; Adamowicz, L. Tautomerism of 2- and 4-thiouracil. Ab initio theoretical study. *J. Am. Chem. Soc.* **1990**, *112*, 1504–1509.
- (38) Rostkowska, H.; Szczepaniak, K.; Nowak, M. J.; Leszczynski, J.; KuBulat, K.; Person, W. B. Thiouracils. 2. Tautomerism and infrared spectra of thiouracils. Matrix-isolation and ab initio studies. *J. Am. Chem. Soc.* **1990**, *112*, 2147–2160.
- (39) Shukla, M. K.; Leszczynski, J. Electronic Transitions of Thiouracils in the Gas Phase and in Solutions: Time-Dependent Density Functional Theory (TD-DFT) Study. *J. Phys. Chem. A* **2004**, *108*, 10367–10375.
- (40) Puzzarini, C.; Biczysko, M.; Barone, V.; Pena, I.; Cabezas, C.; Alonso, J. L. Accurate molecular structure and spectroscopic properties of nucleobases: A combined computational-microwave investigation of 2-thiouracil as a case study. *Phys. Chem. Chem. Phys.* **2013**, *15*, 16965–16975.
- (41) Olsen, J. The CASSCF method: A perspective and commentary. *Int. J. Quantum Chem.* **2011**, *111*, 3267–3272.
- (42) Werner, H.; Knowles, P. J.; Knizia, G.; Manby, F. R.; Schütz, M. Molpro: a general-purpose quantum chemistry program package. *WIREs Comput. Mol. Sci.* **2012**, *2*, 242–253.
- (43) Werner, H.-J.; Knowles, P. J.; Knizia, G.; Manby, F. R.; Schütz, M.; Celani, P.; Korona, T.; Lindh, R.; Mitrushenkov, A.; Rauhut, G.; et al. MOLPRO, version 2012.1, a package of ab initio programs. 2012; see <https://www.molpro.net/>.
- (44) Lischka, H.; Müller, T.; Szalay, P. G.; Shavitt, I.; Pitzer, R. M.; Shepard, R. Columbus - a program system for advanced multireference theory calculations. *WIREs Comput. Mol. Sci.* **2011**, *1*, 191–199.
- (45) Lischka, H.; Shepard, R.; Shavitt, I.; Pitzer, R. M.; Dallos, M.; Müller, T.; Szalay, P. G.; Brown, F. B.; Ahlrichs, R.; Böhm, H. J.; et al. COLUMBUS, an ab initio electronic structure program, release 7.0. 2012.
- (46) Pulay, P. A perspective on the CASPT2 method. *Int. J. Quantum Chem.* **2011**, *111*, 3273–3279.
- (47) Finley, J.; Malmqvist, P.-Å.; Roos, B. O.; Serrano-Andrés, L. The Multi-State CASPT2Method. *Chem. Phys. Lett.* **1998**, *288*, 299.
- (48) Aquilante, F.; De Vico, L.; Ferré, N.; Ghigo, G.; Malmqvist, P.-Å.; Neogrády, P.; Pedersen, T. B.; Pitoňák, M.; Reiher, M.; Roos, B. O.; et al. MOLCAS 7: The Next Generation. *J. Comput. Chem.* **2010**, *31*, 224–247.
- (49) Karlström, G.; Lindh, R.; Malmqvist, P.-Å.; Roos, B. O.; Ryde, U.; Veryazov, V.; Widmark, P.-O.; Cossi, M.; Schimmelpennig, B.; Neogrády, P.; et al. MOLCAS: a program package for computational chemistry. *Comput. Mater. Sci.* **2003**, *28*, 222–239.
- (50) Ghigo, G.; Roos, B. O.; Malmqvist, P.-Å. A modified definition of the zeroth-order Hamiltonian in multiconfigurational perturbation theory (CASPT2). *Chem. Phys. Lett.* **2004**, *396*, 142–149.
- (51) Reiher, M. Relativistic Douglas-Kroll-Hess theory. *WIREs Comput. Mol. Sci.* **2012**, *2*, 139–149.
- (52) Roos, B. O.; Lindh, R.; Malmqvist, P.-Å.; Veryazov, V.; Widmark, P.-O. Main Group Atoms and Dimers Studied with a New Relativistic ANO Basis Set. *J. Phys. Chem. A* **2004**, *108*, 2851–2858.
- (53) Aquilante, F.; Lindh, R.; Bondo Pedersen, T. Unbiased auxiliary basis sets for accurate two-electron integral approximations. *J. Chem. Phys.* **2007**, *127*, 114107.

(54) Schneider, W. C.; Halverstadt, I. F. The Dipole Moments of Thiouracil and Some Derivatives. *J. Am. Chem. Soc.* **1948**, *70*, 2626–2631.

(55) Gozem, S.; Huntress, M.; Schapiro, I.; Lindh, R.; Granovsky, A. A.; Angeli, C.; Olivucci, M. Dynamic Electron Correlation Effects on the Ground State Potential Energy Surface of a Retinal Chromophore Model. *J. Chem. Theory Comput.* **2012**, *8*, 4069–4080.

(56) Barbatti, M.; Ullrich, S. Ionization potentials of adenine along the internal conversion pathways. *Phys. Chem. Chem. Phys.* **2011**, *13*, 15492–15500.

(57) Valsson, O.; Filippi, C. Photoisomerization of Model Retinal Chromophores: Insight from Quantum Monte Carlo and Multi-configurational Perturbation Theory. *J. Chem. Theory Comput.* **2010**, *6*, 1275–1292.

(58) Cremer, D.; Pople, J. A. General definition of ring puckering coordinates. *J. Am. Chem. Soc.* **1975**, *97*, 1354–1358.

(59) Boeyens, J. C. A. The conformation of six-membered rings. *J. Cryst. Mol. Struct.* **1978**, *8*, 317.

(60) Gobbo, J. a. P.; Borin, A. C. On The Population of Triplet Excited States of 6-Aza-2-Thiothymine. *J. Phys. Chem. A* **2013**, *117*, 5589–5596.

(61) Kapur, A.; Steer, R. P.; Mezey, P. G. Ab initio SCF MO calculations of the potential surfaces of thiocarbonyls. III. Ground state and first excited triplet state of thiourea,  $(\text{NH}_2)_2\text{CS}$ . *J. Chem. Phys.* **1979**, *71*, 588–592.

(62) Richter, M.; Mai, S.; Marquetand, P.; González, L. Ultrafast Intersystem Crossing Dynamics in Uracil Unravelling by Ab Initio Molecular Dynamics. *Phys. Chem. Chem. Phys.* **2014**, *16*, 24423.

(63) Milder, S. J.; Kliger, D. S. Spectroscopy and photochemistry of thiouracils: implications for the mechanism of photocrosslinking in tRNA. *J. Am. Chem. Soc.* **1985**, *107*, 7365–7373.

(64) El-Sayed, M. A. Spin-Orbit Coupling and the Radiationless Processes in Nitrogen Heterocyclics. *J. Chem. Phys.* **1963**, *38*, 2834–2838.

(65) Forsberg, N.; Malmqvist, P.-A. Multiconfiguration perturbation theory with imaginary level shift. *Chem. Phys. Lett.* **1997**, *274*, 196–204.

(66) Serrano-Andrés, L.; Merchán, M.; Lindh, R. Computation of conical intersections by using perturbation techniques. *J. Chem. Phys.* **2005**, *122*, 104107.